Electronic Supplementary Material (ESI) for Journal of Materials Chemistry A.
This journal is © The Royal Society of Chemistry 2017

Electronic Supplementary Information

Hierarchical MoP/Ni_2P Heterostructures on Nickel Foam for Efficient Water Splitting

Cuicui Du, Mengxiang Shang, Jianxin Mao and Wenbo Song*

College of Chemistry, Jilin University, Changchun 130012, P.R. China

**E-mail: wbsong@jlu.edu.cn Fax: +86-431-85168420.*

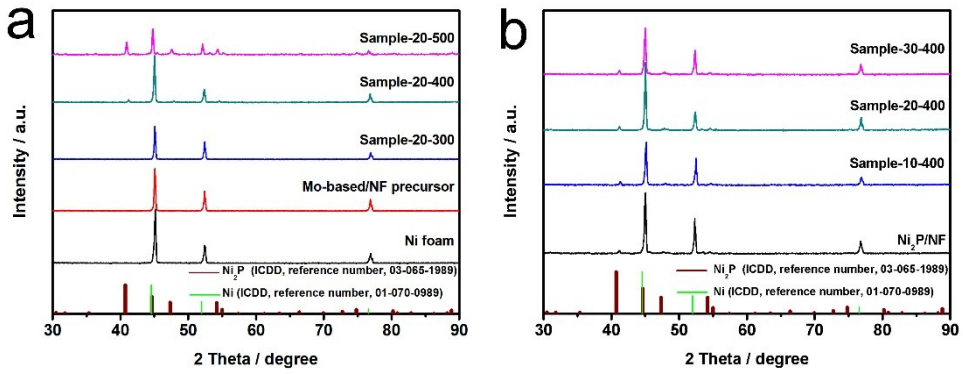

Fig. S1 XRD images for a series of samples synthesized by tuning phosphorization temperature (a) and ammonium molybdate concentration (b).

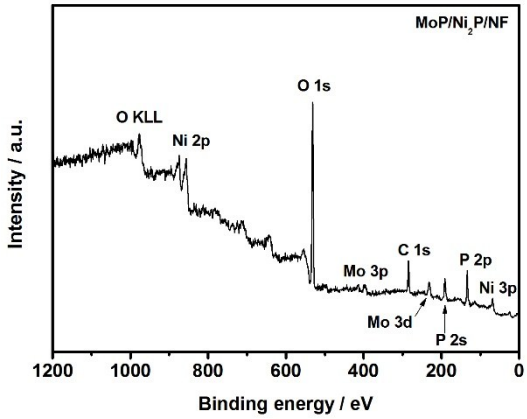

Fig. S2 XPS survey spectrum of $MoP/Ni_2P/NF$.

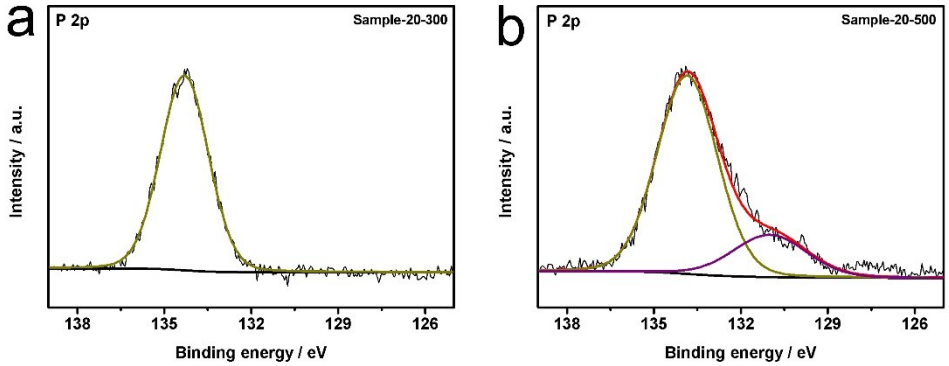

Fig. S3 High resolution XPS spectra of P 2p for sample-20-300 (a) and sample-20-500 (b).

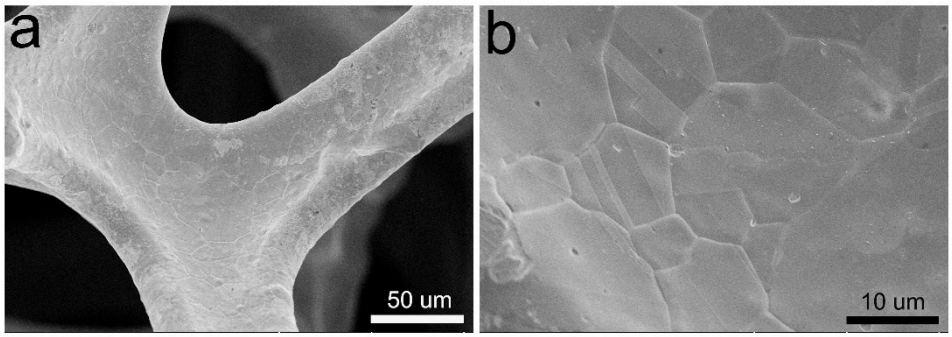

Fig. S4 SEM images of nickel foam (NF).

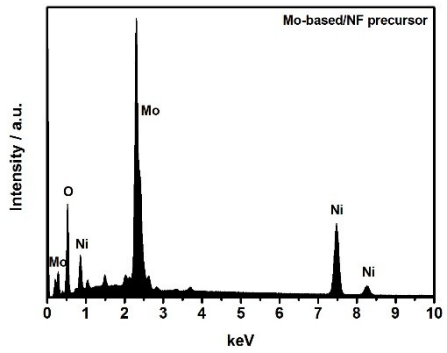

Fig. S5 EDS spectrum of Mo-based/NF precursor

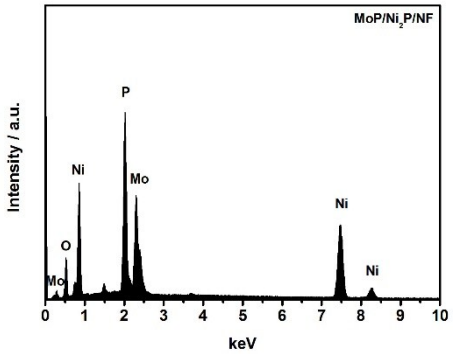

Fig. S6 EDS spectrum of MoP/Ni_2P/NF.

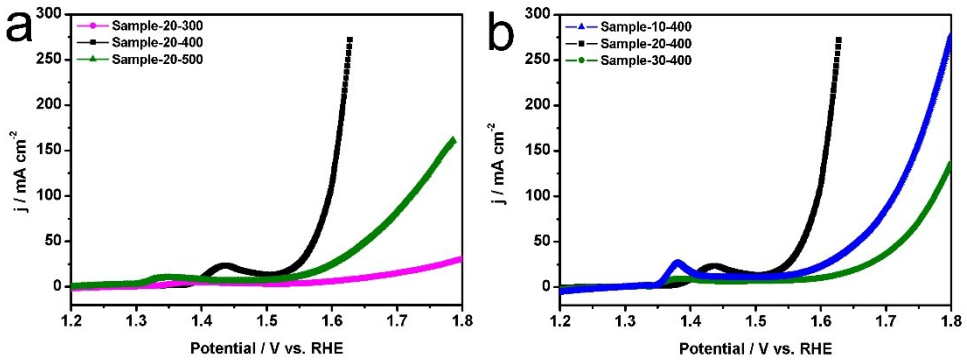

Fig. S7 LSV curves for OER of a series of samples synthesized by tuning phosphorization temperature (a) and ammonium molybdate concentration (b).

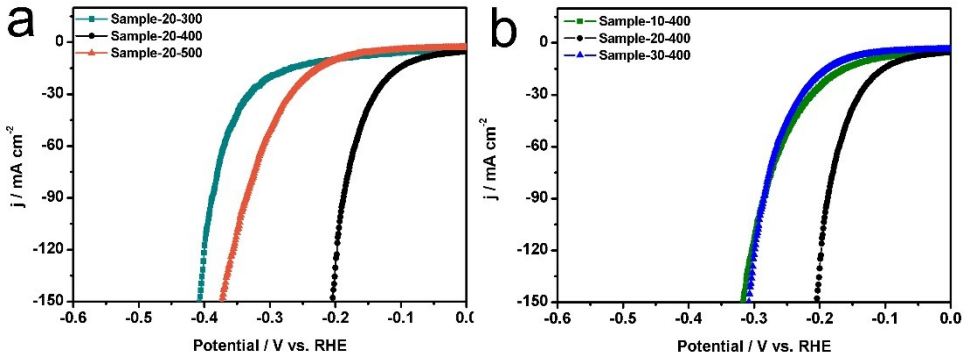

Fig. S8 LSV curves for HER of a series of samples synthesized by tuning phosphorization temperature (a) and ammonium molybdate concentration (b).

The chemical and structural changes of MoP/Ni_2P/NF after a long-term OER or HER tests at a specific potential (j = 10 mV/cm^2) in 1.0 M KOH are performed by XRD, XPS and SEM. The related data is briefly labeled as post-OER MoP/Ni_2P/NF and post-HER MoP/Ni_2P/NF, respectively.

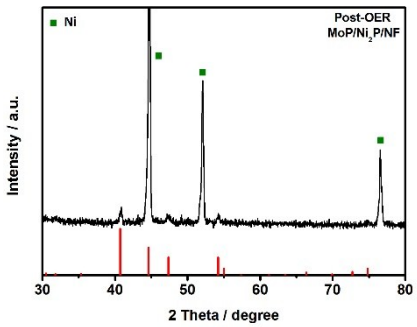

Fig. S9 XRD pattern of post-OER MoP/Ni_2P/NF.

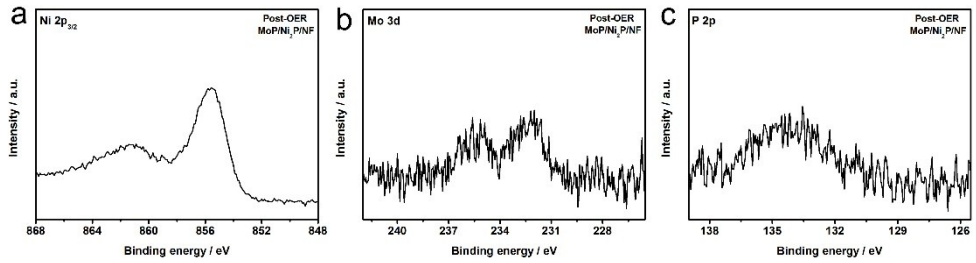

Fig. S10 XPS spectra of Ni $2p_{3/2}$ (a), Mo 3d (b) and P 2p (c) regions of post-OER MoP/Ni_2P/NF.

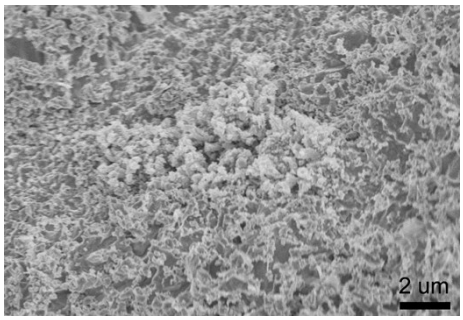

Fig. S11 SEM image of post-OER MoP/Ni_2P/NF.

For OER: The evolution of the crystal structure of MoP/Ni_2P/NF subjected to long-term OER electrolysis is firstly monitored by XRD. Fig. S9 reveals almost identical characteristic diffraction peaks of the material with the MoP/Ni_2P/NF before the OER test (Fig. 2b). The high-resolution XPS spectrum of Ni $2p_{3/2}$ for the post-OER MoP/Ni_2P/NF (Fig. S10a) shows a disappearance of the characteristic peak assignable to $Ni^{\delta+}$ of Ni_2P and an increased intensity of the characteristic peak corresponding to oxidized Ni species, confirming the partial oxidation of Ni_2P after OER test. Similar oxidation phenomenon can also be observed from the high-resolution Mo 3d and P 2p XPS spectra (Fig. S10b-c), evidenced by the disappeared peaks of MoP species. The collective results indicate that the phosphide in MoP/Ni_2P/NF is partially oxidized to oxides/hydroxides/oxyhydroxides on the catalyst surface during the OER under alkaline condition, which is in accordance with the catalytic mechanism of transition metal phosphide for OER in strong alkaline solution.[1-4] Such an oxidative transformation is unavoidable and has been reported previously for a number of other

OER electrocatalysts.[3-12] Fig. S11 displays coarsened and aggregated morphology of the post-OER MoP/Ni_2P/NF. In the centre of the SEM image, one can see that a nanoflower is significantly destroyed and surrounded by many featureless granules. Previous studies also demonstrated the microstructure changes (structural rearrangements) during the OER electrocatalytic process.[4, 8, 13] The OER is a sluggish kinetic reaction operated at high positive potential with continuous evolution of O_2 gas, it is reasonable that changes in morphology might occur especially after a long-term test.[7] It is also worth mentioned that although some structural and compositional transformation happens on the surface during long-term tests, the OER stability is not influenced, as indicated by Fig. 6h, in consist with those of previous reports.[8, 14, 15]

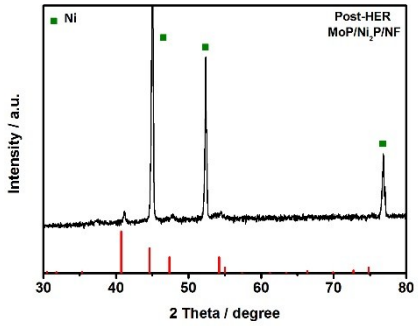

Fig. S12 XRD pattern of post-HER MoP/Ni_2P/NF.

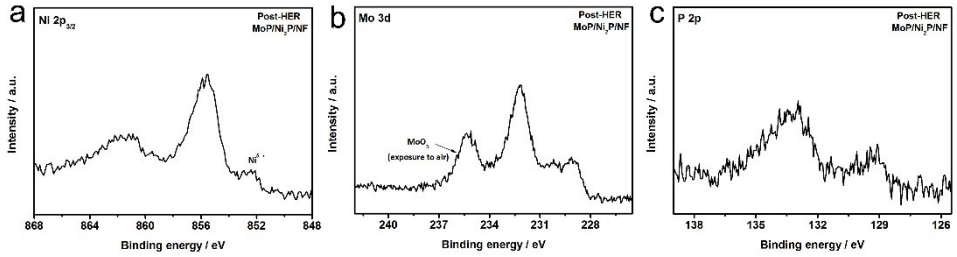

Fig. S13 XPS spectra of Ni $2p_{3/2}$ (a), Mo 3d (b) and P 2p (c) regions of post-HER MoP/Ni_2P/NF.

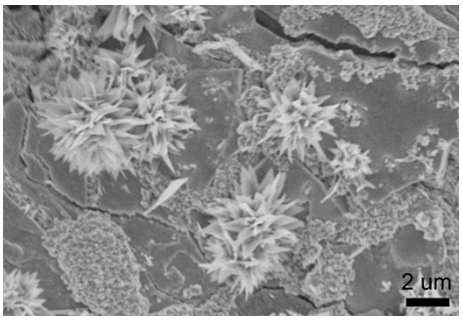

Fig. S14 SEM image of post-HER MoP/Ni_2P/NF.

For HER: The XRD characterization (Fig. S12) demonstrates the presence of Ni_2P composition in the post-HER MoP/Ni_2P/NF, since nearly identical diffraction peaks with those of the as-prepared counterpart (Fig. 2b) are observed. Not much changed high-resolution XPS spectra of Mo, Ni and P (Fig. S13) for the post-HER and the freshly-prepared sample (Fig. 3a, b, e) are also obtained, implying the retention of the electrocatalysts in terms of chemical composition. Additionally, SEM observations on the surface of post-HER MoP/Ni_2P/NF (Fig. S14) suggest the perfect inheritance of the hierarchical structures of the fresh MoP/Ni_2P/NF without any aggregation or damage after recycling usage. Above results corroborate the superior robustness for HER electrocatalysis, which is consistent with its long-term stability for HER (Fig. 7h).

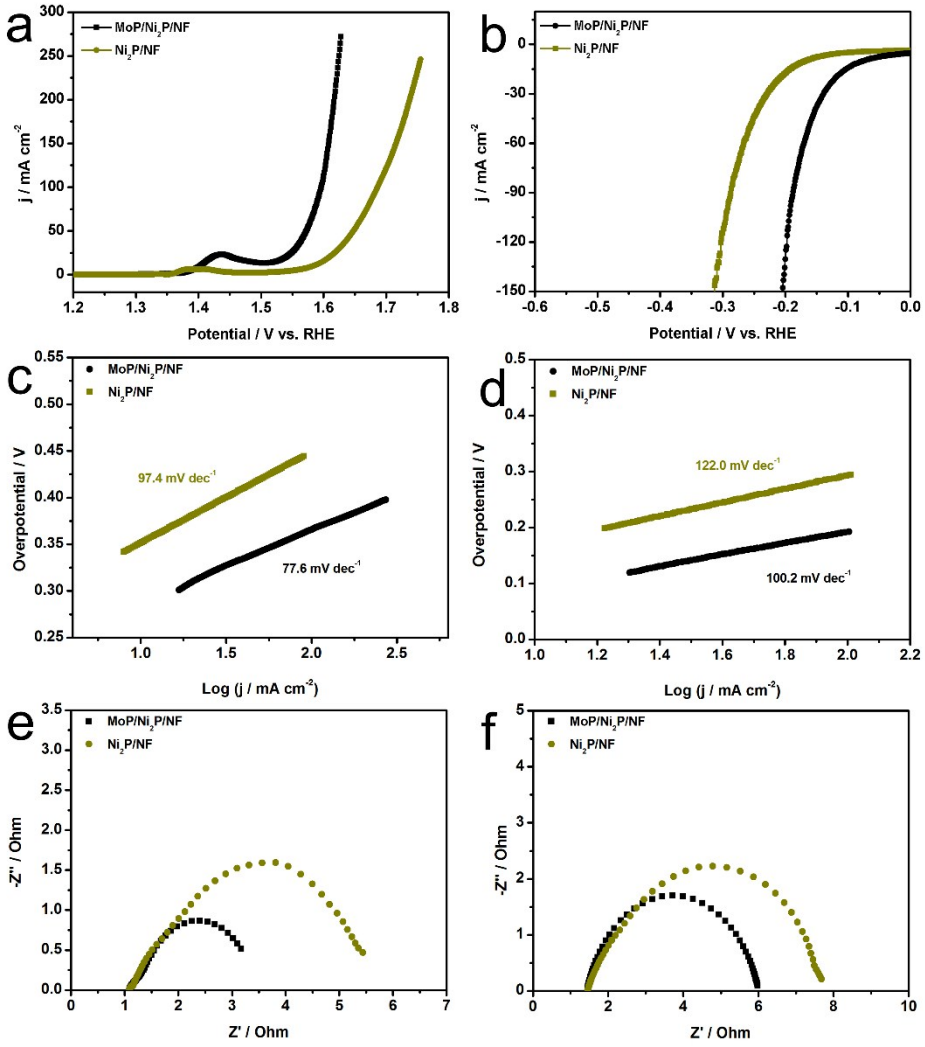

Fig. S15 LSV polarization curves and corresponding Tafel plots for OER (a, c) and HER (b, d); Nyquist plots at overpotential of 340 mV for OER (e) and 200 mV for HER (f).

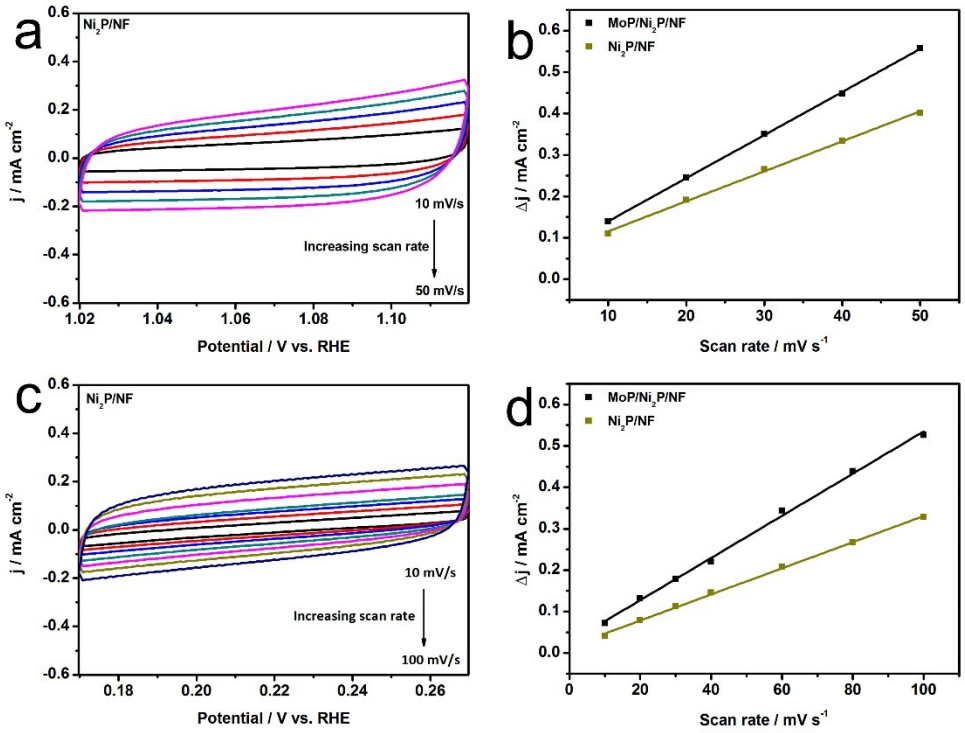

Fig. S16 CVs of Ni_2P/NF for OER (a) and HER(c); Scan rate dependent-current densities at 1.07 V for OER (b) and 0.22 V for HER (d) of Ni_2P/NF and MoP/Ni_2P/NF electrodes.

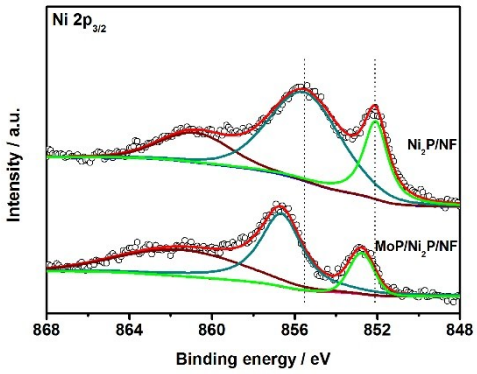

Fig. S17 XPS spectra of Ni $2p_{3/2}$ of MoP/Ni_2P/NF and Ni_2P/NF.

In this work, MoP/Ni_2P/NF shows much enhanced OER and HER activity compared with that of Ni_2P/NF (Fig. S15a-b), suggesting the significance of integrating MoP with Ni_2P for water electrolysis. In order to probe the electron interactions and the possible synergistic effect of MoP and Ni_2P in the hybrid, the Ni $2p_{3/2}$ XPS spectra are investigated. From Fig. S17, the shift of binding energy is clearly observed in the high resolution Ni $2p_{3/2}$ spectrum of MoP/Ni_2P/NF compared to Ni_2P/NF. This result

indicates the existence of strong electronic interactions between MoP and Ni_2P in MoP/Ni_2P/NF.[16-18] Moreover, the electron transfer kinetics and the amount of catalytically active sites of MoP/Ni_2P/NF are compared with those of Ni_2P/NF (Fig. S15e-f, Fig. S16). The MoP/Ni_2P/NF exhibits obviously smaller charge transfer resistance for both OER and HER (Fig. S15e-f). In addition, the two co-existed active phases of MoP and Ni_2P produces more exposed active sites as demonstrated by the CV tests (Fig. S16).[19] Considering the aforementioned results, the improved electrocatalytic activity of MoP/Ni_2P/NF towards OER and HER likely benefits from the synergistic catalytic effect between the bimetallic phosphide of MoP and Ni_2P. The synergistic effect may stem from the strong chemical/electronic coupling between MoP and Ni_2P. The chemical interactions may lead to hierarchical growth of the nanostructures on Ni foam. While the electronic coupling might provide rapid electron transport from catalytic active sites to the electrode.

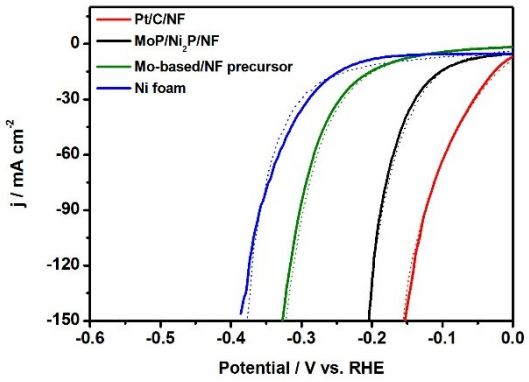

Fig. S18 LSV polarization curves of different electrodes for HER by using a platinum foil (solid lines) and a carbon rod (dashed lines) as the counter electrode.

The HER activity tests of different electrodes has also been performed by using a carbon rod as the counter electrode in 1.0 M KOH. As shown in the Fig. S18, all the electrodes retains almost overlapped polarization curves by using a carbon rod as the counter electrode compared with that of platinum foil counter electrode, indicating that the catalytic activity of the electrodes is not influenced by the counter electrode of Pt foil in 1.0 M KOH.

References

1 Y. J. Bai, L. Fang, H. T. Xu, X. Gu, H. J. Zhang and Y. Wang, *Small*, 2017, **13**, 1603718.

2 J. F. Chang, Y. Xiao, M. L. Xiao, J. J. Ge, C. P. Liu and W. Xing, *ACS Catal.*, 2015, **5**, 6874-6878.

3 J. Ryu, N. Jung, J. H. Jang, H. J. Kim and S. J. Yoo, *ACS Catal.*, 2015, **5**, 4066-4074.

4 L. A. Stern, L. G. Feng, F. Song and X. L. Hu, *Energ. Environ. Sci.*, 2015, **8**, 2347-2351.

5 F. W. Ming, H. F. Liang, H. H. Shi, X. Xu, G. Mei and Z. C. Wang, *J. Mater. Chem. A*, 2016, **4**, 15148-15155.

6 G. F. Chen, T. Y. Ma, Z. Q. Liu, N. Li, Y. Z. Su, K. Davey and S. Z. Qiao, *Adv. Funct. Mater.*, 2016, **26**, 3314-3323.

7 A. Sivanantham, P. Ganesan and S. Shanmugam, *Adv. Funct. Mater.*, 2016, **26**, 4661-4672.

8 X. G. Wang, W. Li, D. H. Xiong and L. F. Liu, *J. Mater. Chem. A*, 2016, **4**, 5639-5646.

9 X. G. Wang, W. Li, D. H. Xiong, D. Y. Petrovykh and L. F. Liu, *Adv. Funct. Mater.*, 2016, **26**, 4067-4077.

10 B. You, N. Jiang, M. L. Sheng, M. W. Bhushan and Y. J. Sun, *ACS Catal.*, 2016, **6**, 714-721.

11 P. W. Menezes, A. Indra, C. Das, C. Walter, C. Gobel, V. Gutkin, D. Schmeisser and M. Driess, *ACS Catal.*, 2017, **7**, 103-109.

12 H. F. Liang, A. N. Gandi, D. H. Anjum, X. B. Wang, U. Schwingenschlogl and H. N. Alshareef, *Nano Lett.*, 2016, **16**, 7718-7725.

13 Z. Y. Zhang, S. S. Liu, J. Xiao and S. Wang, *J. Mater. Chem. A*, 2016, **4**, 9691-9699.

14 S. F. Fu, C. Z. Zhu, J. H. Song, M. H. Engelhard, X. L. Li, D. Du and Y. H. Lin, *ACS Energy Lett.*, 2016, **1**, 792-796.

15 H. W. Huang, C. Yu, C. T. Zhao, X. T. Han, J. Yang, Z. B. Liu, S. F. Li, M. D. Zhang and J. S. Qiu, *Nano Energy*, 2017, **34**, 472-480.

16 X. P. Zhang, L. Huang, Y. J. Han, M. Xu and S. J. Dong, *Nanoscale*, 2017, **9**, 5583-5588.

17 D. Yang, Q. T. Yu, L. Gao, L. Q. Mao and J. H. Yang, *Appl. Surf. Sci.*, 2017, **416**, 503-510.

18 S. Ali, L. Q. Chen, F. L. Yuan, R. Li, T. R. Zhang, S. U. Bakhtiar, X. S. Leng, X. Y. Niu and Y. J. Zhu, *Appl. Catal. B-Environ.*, 2017, **210**, 223-234.

19 G. Zhang, G. C. Wang, Y. Liu, H. J. Liu, J. H. Qu and J. H. Li, *J. Am. Chem. Soc.*, 2016, **138**, 14686-14693.